Title

A hierarchical gray-box dynamic modeling methodology for direct-expansion cooling systems to support control stability analysis

Authors

Liu, Haopeng
Cai, Jie
Kim, Donghun

Publication Date

2022

DOI

10.1016/j.ijrefrig.2021.10.013

Peer reviewed

A hierarchical gray-box dynamic modeling methodology for direct-expansion cooling systems to support control stability analysis

Haopeng Liu[a], Jie Cai[a,*], Donghun Kim[b]

[a]School of Aerospace and Mechanical Engineering, University of Oklahoma, Norman, OK, 73019, USA
[b]Building Technology & Urban Systems Division, Lawrence Berkeley National Laboratory, Berkeley, CA, 94720, USA

Abstract

In this paper, a gray-box dynamic modeling approach for direct-expansion cooling systems is presented. The overall approach incorporates a multi-stage training procedure that consists of 1) identification of component sub-models from quasi-steady-state performance data, 2) system model integration with estimation of refrigerant charge and 3) fine tuning of thermal capacitances of the evaporator and condenser to capture the system dynamic responses. Compared to traditional physics-based models, the proposed modeling approach has advantages including reduced engineering efforts in the model development phase, improved computational efficiency and enhanced prediction accuracy. The modeling method was validated using a 3-ton variable-speed heat pump and proved to be capable of accurately predicting the system transient behaviors over a wide range of operating conditions. The established dynamic model was then applied for control stability analysis, with a specific goal of determining a proper control execution time step. The case study results showed that the stable control execution time step could change significantly, from 3 sec to 19 sec, as the operating conditions and control settings vary, and a proper selection of the execution time step is critical to ensure stable and reliable operations.

Keywords: Gray-box model; multi-stage training; control execution time step; control stability analysis.

Nomenclature

Abbreviations

DX	Direct Expansion
ECM	Electronically Commutated Motor
EXV	Electronic Expansion Valve
HTC	Heat Transfer Coefficient
MB	Moving Boundary
MSS	Minimum Stable Superheat
PI	Proportional Integral
PID	Proportional Integral Derivative
TXV	Thermostatic Expansion Valve
VAV	Variable Air Volume
VCS	Vapor Compression System
VRMSE	Validation Root Mean Square Error
VRMSRE	Validation Root Mean Square Relative Error
ZOH	Zero Order Hold

Greek Numbers

α	heat transfer coefficient (W/K/m^2)
χ_{tt}	Martinelli parameter
$\delta, \hat{\delta}$	piece-wise constant/ discrete time EXV opening (Step)
η_{comb}	combined isentropic efficiency
λ	refrigerant specific heat ratio
ω	compressor speed (RPM)
ρ_f	saturated liquid phase refrigerant density (kg/m^3)
τ	time constant (s)
v_{suc}	specific volume of refrigerant at sucition port (m^3/kg)

Other Symbols

ΔT	control execution time step (s)
ΔT_c	critical execution time step (s)
$\hat{T}_{sh,e}$	discrete-time superheat error (K)
$\hat{T}_{sh,m}$	discrete-time measured superheat (K)
$\hat{T}_{sh,s}$	superheat setpoint (K)

*Corresponding author. Tel.: +1 (405) 325-5390.
Email addresses: Haopeng.Liu-1@ou.edu (Haopeng Liu), jcai@ou.edu (Jie Cai), DonghunKim@lbl.gov (Donghun Kim)

A	heat transfer area (m^2)
C_d	mass flow coefficient
E	tube wall energy (J)
h	enthalpy (J/kg)
K_e	DC gain of surrogate model (K/Step)
K_i	I gain for PI controller (Step/K/sec)
K_p	P gain for PI controller (Step/K)
m	mass flow rate (kg/s)
P	pressure (Pa)
Q	heat transfer rate (W)
q	refrigerant quality
Re	Reynolds number
T	temperature (K)
U	refrigerant internal energy (J)
V	volume (m^3)
T_{sb}	subcooling temperature (K)

Subscripts

a	air side
c	condenser
dis	discharge
e	evaporator
i	inner
l	liquid phase
o	outer
r	refrigerant side
suc	suction
tp	two phase
w	wall

1. Introduction

Vapor compression cycles are predominantly used for air conditioning, heat pump and refrigeration systems, which together consume more than 20% of electricity generated in the U.S. (EIA, 2020) Optimized control is a critical step to achieving maximum energy efficiency, reducing carbon footprint and improving operational reliability of a vapor compression system (VCS). Design of optimal VCS controllers calls for robust dynamic models that can capture system transient behaviors with moderate computational requirements.

Given that the dynamics associated with the heat transfer processes in evaporators and condensers play a dominant role in the overall system transience, dynamic performance characterization of heat exchangers has been a primary focus of prior dynamic modeling efforts, especially on the two-phase flow dynamics which to a large extent affect the evolution of system pressures (Bendapudi and Braun, 2002, Rasmussen, 2012). Catano et al. (2013) proposed a lumped-parameter dynamic model of direct-expansion (DX) systems to facilitate development of gain scheduling controllers. The entire heat exchangers were assumed to operate under two-phase and quasi-steady-state models were adopted for the compressor and electronic expansion valve (EXV). Although the obtained model is computationally efficient with very few governing equations, the lumped approach results in low performance prediction accuracy and is not able to capture important dynamics, e.g., phase transition point oscillations at low superheat. Through division of a heat exchanger according to the different phase regimes, the moving boundary (MB) method seeks to capture the major dynamics of multi-phase heat exchangers while preserving the simplicity of the lumped approach. For example, Chen and Deng (2006) developed a MB-based dynamic model of variable-air-volume DX systems for control analysis, with an empirical heat transfer correlation for each phase regime of the heat exchangers. The nonlinear dynamic features such as hysteresis and dead band were also taken into consideration. The major drawback of the MB method lies on the numerical instability when a single phase region disappears or reappears; to this end, an improved version of the MB approach, termed switched MB, was proposed by Li and Alleyne (2010), which switches between the two-region and one-region model forms for the evaporator by comparing the length of the single-phase region to a pre-determined threshold. A natural extension of the MB approach is the finite control volume method that utilizes a larger number of control volumes to capture system dynamic characteristics at a higher granularity and thus, offers improved model accuracy. Kapadia et al. (2009) presented a finite control volume model of DX air conditioning systems to predict system transient characteristics during system start-up. Beghi and Cecchinato (2009) used a similar finite control volume model to assist design of an auto-tuned PID controller for EXV, where actuation constraints such as upper bound and hysteresis were accounted for explicitly.

Dynamic models have been successfully used for VCS operational stability analysis. Root causes of VCS instability can be classified into two groups: the first is associated with in-

herent characteristics of the two-phase flow in an evaporator or condenser and the second category corresponds to sensing delays (e.g., superheat measurement delays) and improper controller design or settings. The first category is closely related to the concept of minimal stable superheat (MSS) theory , which was first introduced by Huelle (1967) and has been extensively studied since then, e.g., Huelle (1972), Chen et al. (2002, 2008). The MSS is defined as a critical minimal superheat at which the VCS operation becomes unstable; this instability is caused by chattering of the refrigerant-to-tube wall heat transfer coefficient due to mode changes between nucleate boiling and convective boiling. This characteristic is inherent to the evaporation heat transfer process and is not directly related to control actions. The latter category, i.e., control instability of VCS, has attracted significant research interests more recently, mainly driven by the popularization of EXVs and variable-speed drives. Relevant research work addressed the VCS control stability issues from different perspectives, e.g., the impact of the sensing bulb dynamics in a thermal expansion valve-controlled VCS (Eames et al., 2014), design of control gains (Xia and Deng, 2016) and superheat nonlinearity exhibited under different operating conditions (Elliott and Rasmussen, 2010; Xia et al., 2019). For example, Xia and Deng (2016) investigated the influences of proportional–integral (PI) gain settings and superheat sensing dynamics on the operational stability of a DX system, using the Nyquist diagram. Both simulation and experimental results showed that a larger P or I gain would lead to a higher chance of system instability, while a larger superheat sensor time constant has the opposite effect. In a follow-up study (Xia et al., 2019), the authors investigated the effects of superheat sensor dynamics and operating conditions on the operational stability of a DX system, using a dynamic VCS model extended from the one developed by (Chen and Deng, 2006) by adding a sub-model to capture the superheat sensor dynamics. It was found through simulation tests that the increase of the time constant of temperature sensor or the supply fan speed could provide larger stability margins.

This paper presents a multi-stage gray-box dynamic modeling methodology for DX systems to facilitate control stability analysis. A hierarchical training procedure is proposed with separate estimation of the steady-state and dynamic model parameters along with a finite control volume scheme to achieve good model identifiability while ensuring adequate prediction accuracy. Experimental validation of the modeling methodology was conducted using a 3-ton variable-speed heat pump. The developed dynamic model has been utilized for stability analysis of a digital PI controller, with a particular goal of identifying the maximum EXV control execution time step to attain stable operation with minimum EXV lifetime impact. To the authors' knowledge, this is the first attempt in analyzing digital control stability of VCS with respect to control decision time steps.

2. Test unit and experimental setup

The study involves a split variable-speed DX system with a rated cooling capacity of 3 tons to demonstrate the proposed modeling and control analysis approaches. The outdoor unit houses a variable-speed scroll compressor, a condenser coil and a condenser fan, while the indoor unit packages an A-shaped evaporator coil, an (electronic commutated motor) ECM-driven supply fan and an EXV.

In the experimental rig, the indoor unit is connected to an indoor environment test loop, which can accommodate flexible load testing with control accuracies of 0.2°C for dry bulb temperature and ±0.5% for relative humidity. The outdoor unit is located in a psychrometric chamber that can reproduce a wide range of outdoor environmental conditions with identical control accuracies to those of the indoor test loop. The gas and liquid lines connecting the indoor and outdoor units are both approximately 20' long. Details of the experimental setup and the test unit can be found in Liu and Cai (2021a).

3. Modeling methodology

The proposed gray-box modeling methodology consists of a hierarchical training procedure as shown in Figure 1. The bottom layer involves identification of steady-state component models associated with the heat exchangers (evaporator and condenser), compressor and EXV. In the middle layer, the established component models are integrated through continuity equations to obtain a system model in which the refrigerant charge level is estimated by minimizing the mismatch between the predicted and measured steady-state cooling capacity. The top layer transforms the steady-state system model into a dynamic one described by state-space governing equations, in which the optimal thermal capacitances of the heat exchanger walls are identified to best reproduce system transient responses. This hierarchical training methodology minimizes the number (only two) of estimation parameters and the associated numerical iterations of the computationally demanding dynamic model, while the parameters pertinent to steady-state performances (more than ten) are estimated using the fast steady-state models. This hierarchical training approach ensures numerical feasibility for training of the dynamic VCS model. Further, decoupled estimation of parameter groups associated with the different components reduces the risks of over-parameterization and inter-parameter correlations, which is critical for reliable model identification.

The following assumptions are made for the overall modeling approach (Liu and Cai, 2021a)

- Refrigerant-side pressure drops are neglected for both the evaporator and condenser.
- Counter-flow heat exchange is assumed for both heat exchangers.
- Dynamics for the compressor, EXV and air-side energy balances of heat exchangers are neglected.

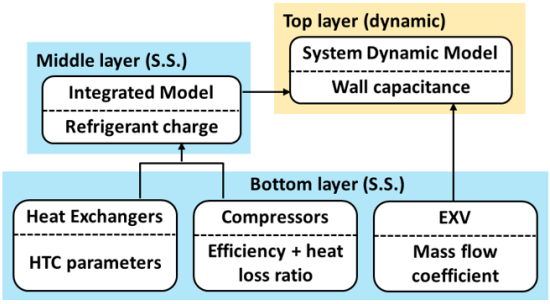

Figure 1: Overall schematic diagram of the gray-box dynamic modeling methodology.

3.1. Steady-state model identification

Identification of the steady-state component and system models, involved in the bottom and middle layers of the hierarchical training procedure, is based on a robust training methodology previously developed by the authors for steady-state characterization of VCSs (Liu and Cai, 2021a). This methodology assumes simplified correlations for the different component models and incorporates two pre-training conditioning steps to improve the model identifiability: (1) a parameter reduction step that identifies and eliminates the non-influential estimation parameters and (2) a parameter de-correlation step where potential correlations among the remaining parameters are identified and reduced, resulting in further estimation parameter reduction. The model structures and key results are summarized in this section for completeness while modeling details can be found in (Liu and Cai, 2021a). The component models capture the component physics through heat and mass balances together with empirical correlations whose parameters are estimated based on performance data. The identified component models are then integrated into a steady-state system model with the refrigerant charge level being the sole estimation parameter.

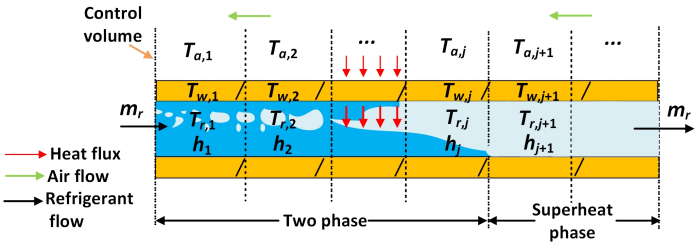

Figure 2: Schematic diagram for a counter-flow, finite control volume model of the evaporator.

3.1.1. Evaporator

A finite control volume approach is adopted for modeling of the evaporator and condenser. A schematic diagram for the evaporator is given in Figure 2. This method divides a heat exchanger into multiple control volumes and characterizes the heat exchange of each control volume according to the local refrigerant and air properties. For the j^{th} control volume, the heat transfer between the air and refrigerant is calculated with the following energy balance equation:

$$Q_j = \alpha_{r,j} A_{i,j} \left(T_{w,j} - T_{r,j}\right) = \alpha_{a,j} A_{o,j} \left(T_{a,j} - T_{w,j}\right) = m_r \left(h_j - h_{j-1}\right) = C_{p,a} m_a \left(T_{a,j+1} - T_{a,j}\right) \quad (1)$$

where Q_j is the heat transfer rate, $\alpha_{r,j}$ and $\alpha_{a,j}$ represent the refrigerant- and air-side HTCs, respectively, $A_{i,j}$ and $A_{o,j}$ are the inner and outer heat transfer areas of the j^{th} section of the exchanger, respectively; $T_{w,j}$, $T_{r,j}$ and $T_{a,j}$ are the tube wall, refrigerant and air temperatures, respectively; $T_{a,j+1}$ and $T_{a,j}$ are the air inlet and outlet temperatures. m_r and m_a are the mass flow rates of the refrigerant and airflow, $C_{p,a}$ is the air specific heat and h_j is the refrigerant enthalpy.

The gray-box evaporator model relies on the following correlation form to estimate the air-side HTC $\alpha_{a,e}$ for a given mass flow rate m_a

$$\alpha_{a,e} A_{o,e} = a_1 m_a^{a_2} \quad (2)$$

where the subscript e stands for evaporator, and a_1 and a_2 are parameters that need to be estimated in the training process.

For estimation of the refrigerant-side evaporation HTC, a simplified form based on the correlation of Chen (1966) is adopted

$$\alpha_{tp,e} = \theta_1 T_e^{\theta_2} \Delta T_{sat}^{\theta_3} \left(\frac{1}{1 + \theta_4 Re_{tp}^{\theta_5}}\right) + \theta_6 \chi_{tt}^{\theta_7} \alpha_{l,e} \quad (3)$$

where θ_1 to θ_7 are the estimation parameters, T_e is the saturated evaporating temperature, ΔT_{sat} is the temperature difference between of the tube wall T_w and T_e, and Re_{tp} is the two-phase Reynolds number. $\alpha_{l,e}$ is the liquid-phase convective HTC obtained using the turbulent flow correlation of Dittus-Boelter (Bergman et al., 1996) and χ_{tt} is the Martinelli parameter which is a function of refrigerant quality q. The two-phase heat transfer dominates the total cooling effect of the evaporator while the cooling effect occurring in the superheated region is relatively minor. Therefore, to improve the model identifiability, the gray-box evaporator model adopts the Gnielinski correlation (Admiraal and Bullard, 1993) for the superheated phase directly, without any training. The void fraction correlation given in Tandon et al. (1985) is adopted to estimate the refrigerant inventory for the evaporator and condenser.

3.1.2. Condenser

The condenser energy balance shares the same form given in Equation 1. The test unit has a fixed-speed condenser fan and therefore, the air-side HTC $\alpha_{a,c}$ is a constant parameter that can be estimated in the training process.

For estimation of the refrigerant condensation HTC $\alpha_{tp,c}$, the following simplified form derived from the Shah correlation (Shah, 1979) is used

$$\alpha_{tp,c} = \alpha_{l,c} \left[c_1 (1-q)^{c_2} + c_3 q^{c_4} T_c^{c_5}\right] \quad (4)$$

where c_1 to c_5 are the estimation parameters, T_c is the saturated condensing temperature, and $\alpha_{l,c}$ is the liquid phase convective HTC. When the quality q approaches zero in Equation 4, the condensation HTC converges to $\alpha_{l,c}$. Therefore, Equation 4

guarantees a smooth HTC transition at the interface between the two-phase and subcooled regions and can capture the heat transfer characteristics for both regions. Similar to the evaporator case, the gray-box model assumes the Gnielinski correlation for the desuperheated region with no training required.

3.1.3. Compressor

The compressor model estimates the refrigerant mass flow rate m_r with

$$m_r = \frac{V_s \cdot \omega}{60 v_{suc}} \tag{5}$$

where v_{suc} is the specific volume of refrigerant at the suction port, ω is the compressor speed (round per minute or RPM), and V_s represents the swept volume of the compressor, which is an estimation parameter. Equation 5 assumes a volumetric efficiency of unity, which is reasonable for scroll compressors (Winandy et al., 2002). For other compressor types, empirical correlations for the volumetric efficiency can be adopted.

The compressor power is modeled based on refrigerant enthalpy gain in a polytropic compression process corrected by a combined isentropic efficiency and a heat loss ratio (Reindl and Klein, 2000):

$$\begin{aligned} Power \cdot (1 - f_{hl})\, \eta_{comb} = m_r \left(h_{dis} - h_{suc}\right) \eta_{comb} = \\ m_r \left\{ \frac{\lambda}{\lambda - 1} P_e v_{suc} \left[\left(\frac{P_c}{P_e} \right)^{\frac{\lambda-1}{\lambda}} - 1 \right] \right\} \end{aligned} \tag{6}$$

where η_{comb} is the combined isentropic efficiency, f_{hl} is the heat loss ratio, h_{dis} and h_{suc} are the discharge and suction enthalpies, respectively, λ is the refrigerant specific heat ratio at the compressor inlet, and P_c and P_e denote the condensing and evaporating pressures, respectively. The following two correlations are used to estimate the compressor isentropic efficiency and heat loss ratio (Chen et al., 2000; Liu and Cai, 2021a):

$$\eta_{comb} = d_1 + d_2 \mathrm{In}\left(\frac{P_c}{P_e}\right) + d_3 \omega + d_4 \mathrm{In}\left(\frac{P_c}{P_e}\right) \cdot \omega \tag{7}$$

$$f_{hl} = e_1 + e_2 \omega + e_3 T_s \tag{8}$$

where d_1 to d_4 and e_1 to e_3 are estimation parameters, and T_s is the outdoor air temperature.

3.1.4. Integrated model

In the bottom layer, the component models described in Section 3.1.1 to Section 3.1.3 are trained separately using quasi-steady-state performance data. In the middle layer, the identified component models are integrated to establish a system model through continuity constraints between the connected components, e.g., the compressor discharge enthalpy of the refrigerant is equal to the condenser inlet enthalpy. Note that the EXV model is not required for steady-state system model integration; instead, an equality is utilized to enforce the predicted superheat to match the measured value. This treatment does not cause accuracy degradation but can reduce the computational complexity of the model training procedure. The model integration stage only involves the identification of the total refrigerant charge level and a simple line search is implemented to find the charge level achieving the minimum root mean square relative error of the total cooling capacity.

3.1.5. Steady-state model accuracy

56 steady-state data points were collected in the laboratory covering a range of operating and control conditions. Out of the 56 steady-state tests, 46 points were used to train the steady-state model and 10 points were utilized for validation. Figure 3 depicts the steady-state system model prediction accuracy against the measurements, where different markers are used to distinguish the training and validation points. The predictions achieve very good agreements with the measurements, with validation root mean square relative errors (VRMSRE) of 3.29% for cooling capacity and 3.86% for compressor power, and with validation root mean square errors (VRMSE) of 0.71K for the saturated evaporating temperature and 0.61K for the saturated condensing temperature. Again, details of the steady-state modeling method can be found in Liu and Cai (2021a).

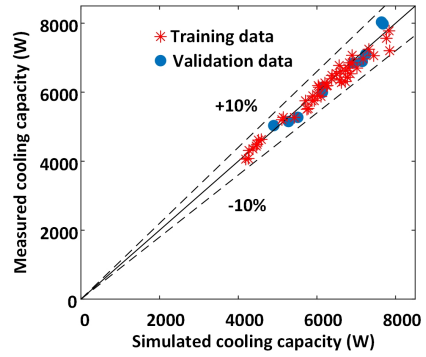

(a)

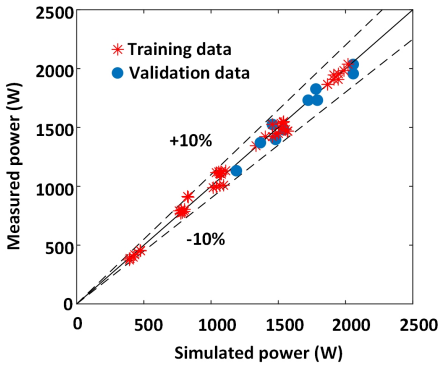

(b)

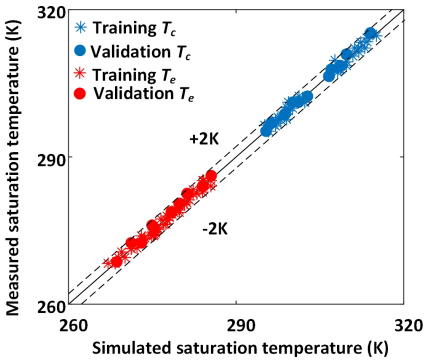

(c)

Figure 3: Comparisons of system model predictions and experimental results for (a) cooling capacity (VRMSRE=3.29%), (b) power consumption (VRMSRE=3.86%) and (c) saturation temperatures (VRMSE=0.71K for T_e and VRMSE=0.61K for T_c).

3.2. Dynamic model identification

3.2.1. EXV model

EXVs are increasingly used in modern VCS because of their fast and accurate response to control actuation and adaptability to time-varying operating conditions. An EXV model is not required in the steady-state model as the measured superheat is used as an input variable. However, a dynamic VCS model ought to characterize the dynamics of superheat (an output variable) and should incorporate an EXV model. This study assumes the following orifice equation to calculate the refrigerant flow through the EXV (Li, 2013)

$$m_r = C_d A Y \sqrt{2\rho_f \left(P_c - P_e\right)} \tag{9}$$

where A is the throat area of the EXV when it's fully open and ρ_f is the saturated liquid refrigerant density at the condensing pressure. Y is the expansion factor capturing volume expansion of the refrigerant when two-phase refrigerant enters the EXV; the expansion factor is dependent on the refrigerant pressure ratio and thermal properties, e.g., specific heat (Davies and TC, 1973). When sub-cooled refrigerant enters the EXV (i.e., subcooling is nonzero), the expansion factor is unity. The mass flow coefficient C_d is a dimensionless variable that changes with the valve opening δ and subcooling T_{sb}. The following polynomial is found appropriate to capture the EXV behavior from the experimental data:

$$C_d = f_1 + f_2\delta + f_3\delta^2 + f_4\delta\left(\frac{T_{sb}}{T_c}\right) \tag{10}$$

where T_c is the critical temperature of the refrigerant, and f_1 to f_4 are estimation parameters.

Figure 4 shows the EXV model performance, with the same training and validation data sets. The model is able to predict the refrigerant mass flow rate with a VRMSRE of less than 7%. The prediction error is higher than those of the other component models, due to higher uncertainties in the OEM EXV characteristics: small offsets in the refrigerant mass flow were observed across multiple repeated tests with exactly the same control and operation settings. Despite the uncertainty, the overall EXV mass flow prediction is still satisfactory.

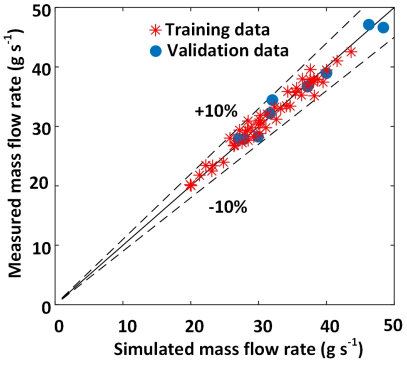

Figure 4: Comparison of predicted and measured refrigerant mass flow rate through the EXV (VRMSRE=6.95%).

3.2.2. Dynamic heat exchanger model

The evaporator dynamic model extends the steady-state one by incorporating explicit conservation differential equations for the refrigerant energy, mass and tube wall energy of each control volume, given in Equation 11 to Equation 13.

$$\dot{U}_j = m_{j-1}h_{j-1} - m_j h_j + \alpha_{r,j}A_{i,j}\left(T_{w,j} - T_{r,j}\right) \tag{11}$$

$$\dot{m}_{e,j} = m_{j-1} - m_j \tag{12}$$

$$\begin{aligned}\dot{E}_j = \left(C_{th,w}\right)_j \dot{T}_{w,j} =& \alpha_{a,j}A_{o,j}\left(T_{a,j} - T_{w,j}\right) \\ &- \alpha_{r,j}A_{i,j}\left(T_{w,j} - T_{r,j}\right)\end{aligned} \tag{13}$$

where U_j is the refrigerant internal energy; m_{j-1} and m_j represent the inlet and outlet mass flow rates of refrigerant, respectively; $\dot{m}_{e,j}$ is the time derivative of the refrigerant mass held

in the j^{th} control volume; E_j is the tube wall energy and $C_{th,w}$ denotes the thermal capacitance of the heat exchanger tube wall, which is estimated in the training process. The HTCs and areas assume the values identified in the bottom and middle layers so the evaporator dynamic model only involves a single estimation parameter.

Based on the relationship between the refrigerant specific internal energy u and enthalpy ($u = h - \frac{P}{\rho}$), the time derivative of the refrigerant internal energy in Equation 11 can be decomposed into terms of time derivatives with respect to the pressure and enthalpy using the chain rule:

$$\dot{U}_j = V_j \left[\left(\frac{\partial \rho_j}{\partial P_e}\bigg|_{h_j} \right) \dot{P}_e + \left(\frac{\partial \rho_j}{\partial h_j}\bigg|_{P_e} \right) \dot{h}_j \right] h_j - V_j \dot{P}_e + V_j \rho_j \dot{h}_j \tag{14}$$

where V_j represents the tube internal volume for the j^{th} control volume and the evaporating pressure P_e is assumed to be identical across all control volumes (no pressure drops). Similarly, the mass balance Equation 12 can be re-written as

$$\dot{m}_{e,j} = V_j \dot{\rho}_j = V_j \left[\left(\frac{\partial \rho_j}{\partial P_e}\bigg|_{h_j} \right) \dot{P}_e + \left(\frac{\partial \rho_j}{\partial h_j}\bigg|_{P_e} \right) \dot{h}_j \right] \tag{15}$$

Equation 14 and Equation 15 allow the following reformulation of the governing equations using the evaporation pressure and enthalpy as state variables:

$$\mathbf{Z} \begin{bmatrix} \dot{P}_e \\ \dot{h}_1 \\ \vdots \\ \dot{h}_N \\ \dot{T}_{w,1} \\ \vdots \\ \dot{T}_{w,N} \end{bmatrix} = \begin{bmatrix} m_{in}\left(h_{in} - h_1\right) + \alpha_{r,1} A_{i,1}\left(T_{w,1} - T_{r,1}\right) \\ \vdots \\ m_{in}\left(h_{N-1} - h_{out}\right) + \alpha_{r,N} A_{i,N}\left(T_{w,N} - T_{r,N}\right) \\ m_{in} - m_{out} \\ \alpha_{a,1} A_{o,1}\left(T_{a,1} - T_{w,1}\right) - \alpha_{r,1} A_{i,1}\left(T_{w,1} - T_{r,1}\right) \\ \vdots \\ \alpha_{a,N} A_{o,N}\left(T_{a,N} - T_{w,N}\right) - \alpha_{r,N} A_{i,N}\left(T_{w,N} - T_{r,N}\right) \end{bmatrix} \tag{16}$$

where $\mathbf{Z}$ is the transformation matrix that is dependent on the evaporation pressure and refrigerant enthalpy of each control volume. The detailed structure of the matrix can be found in Gupta (2007). N denotes the total number of control volumes. m_{in} and m_{out} are the inlet and outlet refrigerant mass flow rates for the evaporator, respectively. Solving the nonlinear differential Equation 16 requires inversion of the transformation matrix, the size of which depends on the number of dynamic state variables ($2N+1$). The computational complexity for (non-sparse) matrix inversion increases cubically with N, i.e., $O(N^3)$. In the case study, to seek a trade-off between the model accuracy and computational efficiency, the evaporator was divided into 20 control volumes, i.e., $N = 20$. The differential equations were solved numerically using the fourth-order Runge-Kutta solver with a fixed time step of 0.05 s (Greenberg, 1988).

The governing equations for the condenser dynamics assume exactly the same form, although a different tube wall thermal capacitance is identified through training.

3.2.3. Dynamic system model

In addition to the integration of the EXV model, the VCS dynamic system model is an natural extension of the steady-state system model established in the middle layer, by incorporating the governing differential equations for the evaporator and condenser dynamics introduced in Section 3.2.2. Since the dynamics of the compressor and EXV are fast and negligible compared to those of the heat exchangers, their steady-state models carry over directly to the dynamic system model. The dynamic system model is established by connecting the component models in a ping-pong scheme: the output of an upstream component for the previous time step is used as the input to calculate the current state of the downstream component. Mass balance is always preserved in the governing differential equations. However, an initialization step is needed to estimate the initial values of the state variables through trial and error so that the total system refrigerant charge of the dynamic model matches the charge level estimated for the steady-state counterpart in the middle layer.

As part of identification of the dynamic system model, thermal capacitances of the heat exchanger tube walls are estimated so that the predicted superheat matches the experimental data with the minimum RMSRE. Superheat is used as the regression variable since superheat stability is a key requirement for controller design of variable-speed VCS.

To illustrate the impact of heat exchanger thermal capacitances on the overall system dynamics, the comparisons between the predicted superheat with different evaporator thermal capacitance values and the measured superheat for the test unit are shown in Figure 5, where $C_{th,r}$ denotes the reference evaporator tube wall thermal capacitance calculated from detailed coil geometries provided by the manufacturer. The estimated thermal capacitance is 30% higher than the reference value, possibly because the model also tends to capture the thermal inertia of the temperature sensor (thermocouple installed in the suction line with a metal sheath). The estimated thermal capacitance leads to transient behaviors in best agreement with the measured dynamics. It can be seen from Figure 5 that a small thermal capacitance ($0.5C_{th,r}$) leads to fast responses while a large capacitance ($2C_{th,r}$) results in slow system dynamics.

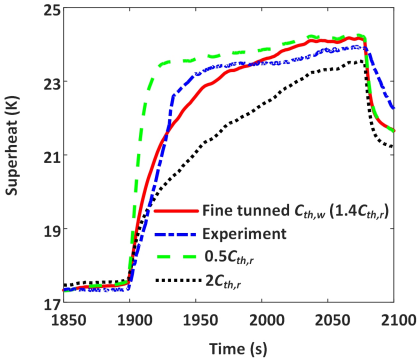

Figure 5: Comparisons of superheat dynamics associated with different evaporator thermal capacitance values.

3.2.4. *Dynamic system model accuracy*

The final dynamic system model was validated with experimental data collected in a continuous test that consisted of a sequence of different operation settings. The comparisons of the measured and predicted cooling capacity, compressor power consumption, evaporator/condenser saturation temperatures and superheat are depicted in Figure 6. The results demonstrate that the identified dynamic model could accurately capture the system dynamics. For this specific validation data set, the model prediction RMSREs are 1.1% for cooling capacity, 3.7% for compressor power consumption, less than 0.8K for the saturated evaporation/condensation temperatures and 0.9K for the superheat.

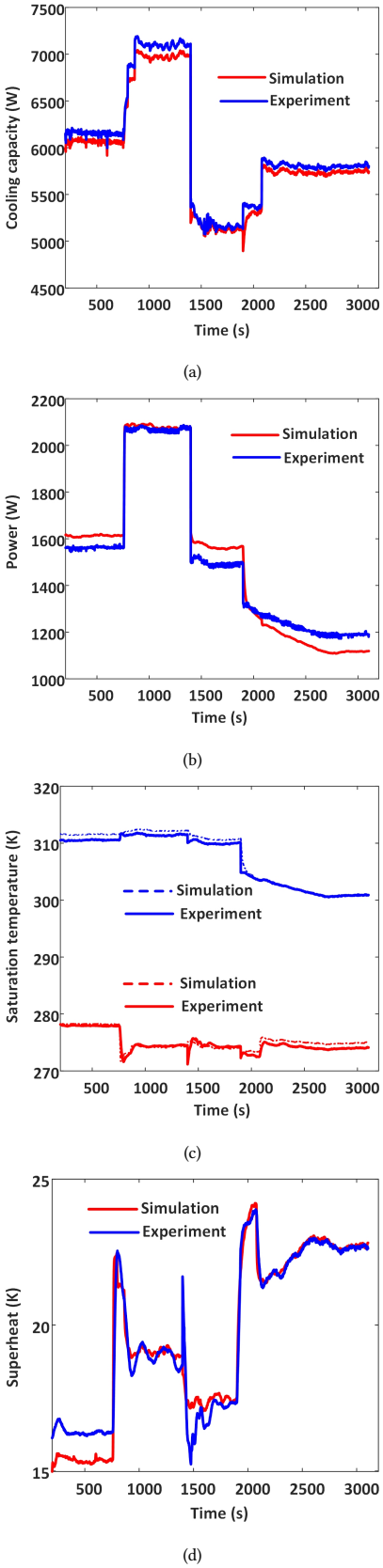

Figure 6: Comparisons of system dynamic performance between simulation and experiment for (a) cooling capacity (RMSRE=1.67%), (b) power consumption (RMSRE=3.69%), (c) saturation temperatures (RMSE=0.73K for T_e and RMSE=0.64K for T_c) and (d) superheat (RMSE=0.87K).

4. Application of the dynamic model for control analysis

This section presents an application of the developed VCS dynamic model for control analysis, with a specific focus on the determination of proper EXV control execution time steps. For a given feedback controller (e.g., proportional–integral-derivative or PID controller), a short execution time step could provide fast and accurate superheat regulation but frequent actuation may reduce the lifetime of the valve and stepper motor; on the other hand, an excessively large execution time step setting can lead to control instability such as superheat hunting which may trigger control oscillations of both the EXV and compressor. Therefore, a proper setting of the control execution time step is critical to ensure reliable and efficient VCS operations.

4.1. Transfer function of PI controlled VCS

This study considers a digital PI controller for superheat regulation, which is predominantly used for industrial process control. However, the analysis method presented here is applicable to general linear feedback controllers. Figure 7 shows the block diagram of the digital superheat control loop, where the PI controller accepts the superheat control error $\hat{T}_{sh,e}$ between the superheat setpoint $\hat{T}_{sh,s}$ and the measured superheat $\hat{T}_{sh,m}$, and generates the control command $\hat{\delta}$ for the EXV opening. The PI controller has the following discrete-time transfer function:

$$C(z) = \frac{\mathscr{Z}\{\hat{\delta}\}}{\mathscr{Z}\{\hat{T}_{sh,e}\}} = K_p + K_i \frac{\Delta T z}{z-1} \tag{17}$$

where K_p and K_i are the proportional and integral gains, respectively, ΔT is the execution time step of the controller, and $\mathscr{Z}$ is the Z-transform operator. Note that throughout this paper, a continuous-time signal is denoted by a regular variable while a discrete-time (sampled) signal is represented by a hatted variable.

The continuous-time transfer function of the VCS plant model is denoted by $H(s)$. Zero-order hold (ZOH) is applied to the discrete-time control command $\hat{\delta}$ generated by the PI controller to reconstruct a continuous-time and piece-wise constant signal δ fed to the VCS plant. The ZOH operator has the following transfer function (Landau and Zito, 2007)

$$K(s) = \frac{\mathscr{L}\{\hat{\delta}\}}{\mathscr{L}\{\delta\}} = \frac{1-\mathrm{e}^{-s\Delta T}}{s} \tag{18}$$

where $\mathscr{L}$ is the Laplace-transform operator. A sampler is present after the VCS plant to obtain a discrete-time superheat signal ($\hat{T}_{sh,m}$). The discrete-time equivalent VCS plant model with the ZOH process is represented by $KH(z)$.

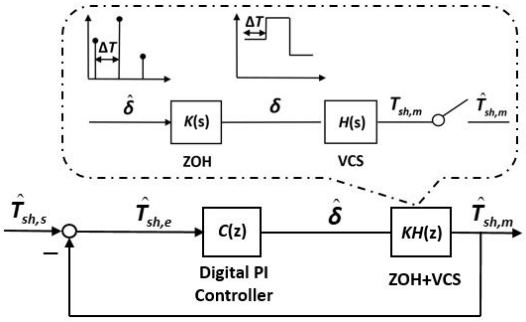

Figure 7: Block diagram of the digital superheat controller.

The original VCS plant model is highly nonlinear and thereby not suitable for control analysis. To this end, a linear surrogate model is derived for given operating conditions from step response tests conducted with the original VCS model. Based on the test results reported in Liu and Cai (2021b), a first-order surrogate model is assumed (this is a common assumption by prior work, e.g., Rasmussen, 2012):

$$H(s) = \frac{\mathscr{L}\{T_{sh,m}\}}{\mathscr{L}\{\delta\}} = \frac{K_e}{1+\tau s} \tag{19}$$

where τ is the time constant and K_e is the DC gain of the surrogate model, which is equal to the variation of the steady-state superheat subject to a unit step change in the EXV opening. Note that both the time constant and the DC gain change with operating conditions and the analysis results are only valid for the conditions under which the surrogate model is developed. When the operation conditions change, the surrogate model ought to be updated. The discrete-time equivalent model of the VCS plant with the ZOH process is:

$$KH(z) = \frac{\mathscr{Z}\{\hat{T}_{sh,m}\}}{\mathscr{Z}\{\hat{\delta}\}} = \frac{K_e\left(1-\mathrm{e}^{-\frac{\Delta T}{\tau}}\right)}{z-\mathrm{e}^{-\frac{\Delta T}{\tau}}} \tag{20}$$

Then, the closed-loop discrete-time transfer function for the superheat control system is:

$$G(z) = \frac{\mathscr{Z}\{\hat{T}_{sh,m}\}}{\mathscr{Z}\{\hat{T}_{sh,s}\}} = \frac{C(z)\,KH(z)}{1+C(z)\,KH(z)} = \frac{Bz+D}{z^2+Ez+F} \tag{21}$$

where

$$\begin{aligned}
B =& K_e\left(K_p + K_i\Delta T\right)\left(1-\mathrm{e}^{-\frac{\Delta T}{\tau}}\right),\\
D =& -K_eK_p\left(1-\mathrm{e}^{-\frac{\Delta T}{\tau}}\right),\\
E =& K_e\left(K_p + K_i\Delta T\right)\left(1-\mathrm{e}^{-\frac{\Delta T}{\tau}}\right) - \left(1+\mathrm{e}^{-\frac{\Delta T}{\tau}}\right),\\
F =& \mathrm{e}^{-\frac{\Delta T}{\tau}} - K_eK_p\left(1-\mathrm{e}^{-\frac{\Delta T}{\tau}}\right).
\end{aligned}$$

Discrete-time closed-loop stability can be guaranteed if all the closed-loop poles, which are the roots of the characteristic equation $z^2 + Ez + F$, fall within the unit circle in the z-plane (Fadali and Visioli, 2013). This stability criterion is used to analyze the effect of control execution time step ΔT on system stability.

4.2. Case study results on control stability

4.2.1. Surrogate model-informed stability

Figure 8 depicts the variation of the distance between the dominant pole of the closed-loop system and the origin of the z-plane with respect to the control execution time step, under different P/I gain settings. The analysis corresponds to the following boundary conditions: evaporator inlet air dry-bulb temperature of 305K and relative humidity of 35%, outdoor air dry-bulb temperature of 300K, compressor speed at 3000 RPM and supply air flow rate of 1200 CFM. The Ziegler–Nichols rule (Katsuhiko, 2010) was used to fine tune the P/I gains with the full VCS model under the same operating conditions. The P/I gains were determined to be 2 (Step/K) and 0.09 (Step/K/sec), respectively. Open-loop simulation tests were conducted under the same conditions and the results were utilized for estimation of the surrogate model, the time constant τ and DC gain K_e of which were identified to be 41.5 s and 7.112 (K/Step), respectively. The results presented in Figure 8 were obtained using the estimated surrogate model for the specific boundary conditions. It can be observed that for all considered P/I gain settings, the dominant pole's distance from the origin increases monotonically with the increase of the control execution time step and when the control time step reaches certain threshold, the closed-loop pole crosses the unit circle and the system becomes unstable. This threshold is termed critical execution time step ΔT_c, which is a critical parameter to consider in the design of a digital controller: the control time step needs to be smaller than this threshold to maintain stability of the closed-loop system. Another key observation is that the critical time step varies dramatically with the P/I gain settings: the increase of the P or I gain, which corresponds to more aggressive control reactions to superheat errors, leads to a decrease of ΔT_c. This is expected as more frequent control actuation is needed to accommodate the dramatic changes in the control command by an aggressive PI controller.

To investigate the effect of operating conditions on the critical time step, analyses were performed for a different set of boundary conditions: the evaporator inlet/outdoor air conditions remained the same as those in Figure 8 but the compressor speed and supply air flow rate were changed to 3500 RPM and 1800 CFM, respectively. The results are depicted in Figure 9. The VCS response is quite different under the new boundary conditions and the surrogate VCS model was re-identified accordingly. The updated surrogate model has a slightly larger time constant and a significantly smaller DC gain. Although the curves exhibit similar trends, the critical time step ΔT_c has changed quite significantly as a consequence of the variation in system dynamics. For the nominal P/I gain settings of 2 (Step/K) and 0.09 (Step/K/sec), the critical time step has increased from 6.09 s to 9.45 s after the changes in the boundary conditions. These results indicate the promise of an improved strategy to adapt the control execution time step with the operating conditions, which can offer benefits of reducing control actuation and prolonging equipment lifetime with guaranteed stability. However, this is out of the scope of this study.

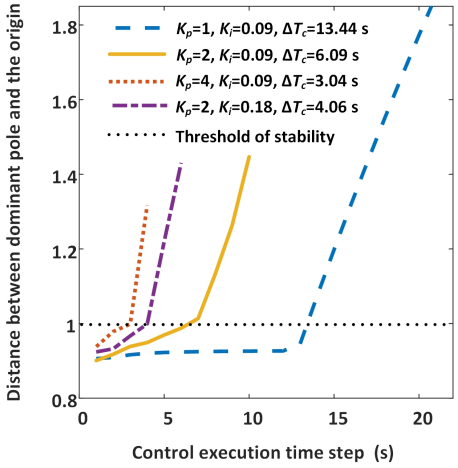

Figure 8: Variation of distance between dominant pole and the origin with respect to the control execution time step for τ = 41.5s, K_e = 7.112K/Step.

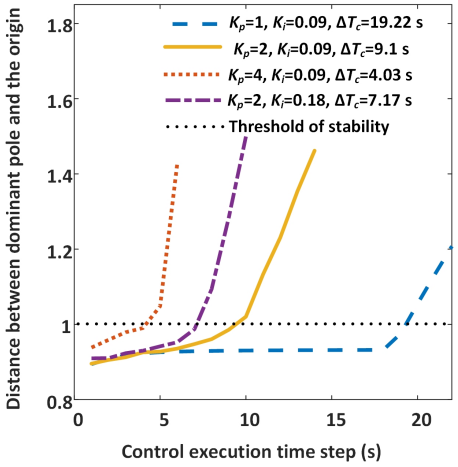

Figure 9: Variation of distance between dominant pole and the origin with respect to the control execution time step for τ = 36.5s, K_e = 3.875K/Step.

4.2.2. Experimental validation of the stability results

Experimental tests were carried out using the test unit to validate the stability results presented in the previous subsection. The test assumed the same operating conditions as those in Figure 8 and the nominal P/I gains of 2 (Step/K) and 0.09 (Step/K/sec). In the experiments, all boundary conditions and P/I gains remained constant while the PI controller execution time step was gradually increased from 2 s to 14 s with a 2 s increment. Each execution time step setting lasted 30 minutes to ensure the system reached steady- or oscillatory-steady-state before the next setting was applied.

Figure 10 presents the experimental results. It can be observed that the system was stable for controller execution time steps shorter than 6 s, while unstable superheat oscillations occurred when ΔT was increased to 8 s and the control response became more oscillatory as ΔT was further increased. These results are consistent with the critical execution time step of 6.09 s, identified in the stability analysis of Section 4.2.1. The dominant pole's distance from the origin is indicated for each

execution time step setting in the first subplot of Figure 10, which also proves that ΔT of 6 s is very close to the stability threshold with the dominant pole almost falling on the unit circle. It may be noted that a larger control execution time step is anticipated to reduce mechanical wear and tear of the valve and stepper motor. However, an excessively large control time step may cause system instability and control chattering which can even accelerate the aging of the expansion device, as evidenced by the results in Figure 10.

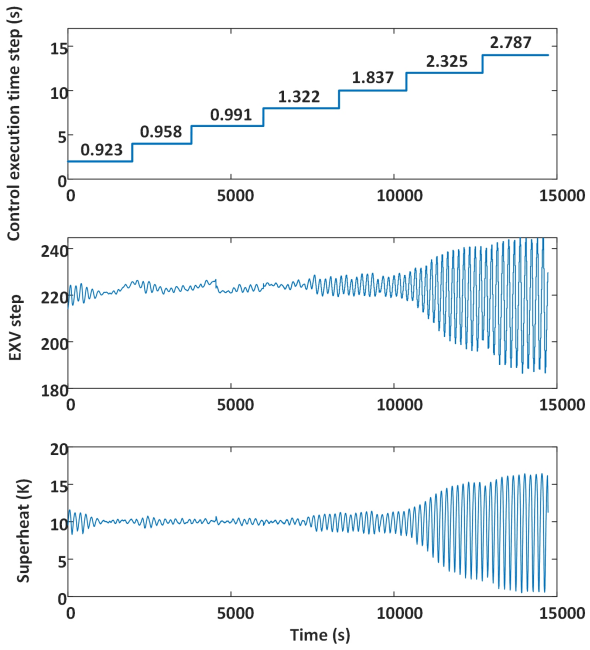

Figure 10: Experimental results under different control execution time step.

5. Conclusions

This paper presented a multi-layer gray-box dynamic modeling methodology for vapor compression systems, which achieves superb model estimation efficiency and reliability by decomposing the model estimation task into multiple sub-problems that can be addressed separately. The performance of the methodology was demonstrated using performance data collected from a 3-ton variable-speed heat pump test unit. The test results verified that the established model can provide accurate predictions of both steady-state and dynamic behaviors under a range of operating conditions. The application of the established dynamic model for digital control stability analysis was presented and the case study results showed that the stability threshold for the PI control execution time step varies significantly with the operating conditions and P/I gain settings. This finding motivates the development of an improved control scheme to adapt the control execution time step with operating conditions, which can significantly reduce valve control actuation with guaranteed stability. This will be investigated in future work.

References

D. M. Admiraal and C. W. Bullard. Heat transfer in refrigerator condensers and evaporators. *Air Conditioning and Refrigeration Center. College of Engineering. University of Illinois at Urbana-Champaign*, 1993.

A. Beghi and L. Cecchinato. A simulation environment for dry-expansion evaporators with application to the design of autotuning control algorithms for electronic expansion valves. *International Journal of Refrigeration*, 32(7): 1765–1775, 2009.

S. Bendapudi and J. E. Braun. Development and validation of a mechanistic, dynamic model for a vapor compression centrifugal liquid chiller. *Report of ASHRAE*, 2002.

T. L. Bergman, F. P. Incropera, D. P. DeWitt, and A. S. Lavine. *Fundamentals of heat and mass transfer*. Wiley, 1996.

J. Catano, F. Lizarralde, T. Zhang, J. T. Wen, M. K. Jensen, and Y. Peles. Vapor compression refrigeration cycle for electronics cooling–part ii: gain-scheduling control for critical heat flux avoidance. *International Journal of Heat and Mass Transfer*, 66:922–929, 2013.

J. C. Chen. Correlation for boiling heat transfer to saturated fluids in convective flow. *Industrial engineering chemistry process design and development*, 5(3):322–329, 1966.

W. Chen and S. Deng. Development of a dynamic model for a dx vav air conditioning system. *Energy Conversion and Management*, 47(18-19):2900–2924, 2006.

W. Chen, C. Zhijiu, Z. Ruiqi, and W. Yezheng. A study on the operational stability of a refrigeration system having a variable speed compressor. *International Journal of Refrigeration*, 25(8):1137–1142, 2002.

Y. Chen, N. P. Halm, E. A. Groll, and J. E. Braun. A comprehensive model of scroll compressors part ii: overall scroll compressor modeling. 2000.

Y. Chen, S. Deng, X. Xu, and M. Chan. A study on the operational stability of a refrigeration system having a variable speed compressor. *International Journal of Refrigeration*, 31(8):1368–1374, 2008.

A. Davies and D. TC. Single and two-phase flow of dichlorodifluoromethane,(r12), through sharp-edged orifices. volume 79, pages 109–123, 1973.

I. W. Eames, A. Milazzo, and G. G. Maidment. Modelling thermostatic expansion valves. *International journal of refrigeration*, 38:189–197, 2014.

EIA. Electricity data. 2020. u.s. https://www.eia.gov/ energyexplained/ electricity/use-of-electricity.php, 2020.

M. S. Elliott and B. P. Rasmussen. On reducing evaporator superheat nonlinearity with control architecture. *International journal of refrigeration*, 33(3): 607–614, 2010.

M. S. Fadali and A. Visioli. *Digital control engineering: analysis and design*. Academic Press, 2013.

M. D. Greenberg. *Advanced engineering mathematics*. Prentice Hall, 1988.

A. Gupta. Reduced order modeling of heat exchangers using high order finite control volume models. Master's thesis, 2007.

Z. R. Huelle. Heat load influences upon evaporator parameters. volume 2 of *12th International Refrigeration Congress*, pages 985–1002, 1967.

Z. R. Huelle. Mss line-new approach to hunting problem. *ASHRAE JOURNAL-AMERICAN SOCIETY OF HEATING REFRIGERATING AND AIR-CONDITIONING ENGINEERS*, 14(10):43–46, 1972.

R. G. Kapadia, S. Jain, and R. S. Agarwal. Transient characteristics of split air-conditioning systems using r-22 and r-410a as refrigerants. *HVACR Research*, 15(3):617–649, 2009.

O. Katsuhiko. *Modern control engineering*. Prentice Hall, 2010.

I. D. Landau and G. Zito. *Digital control systems: design, identification and implementation*. Springer Science Business Media, 2007.

B. Li and A. G. Alleyne. A dynamic model of a vapor compression cycle with shut-down and start-up operations. *International Journal of Refrigeration*, 33(3):538–552, 2010.

W. Li. Simplified modeling analysis of mass flow characteristics in electronic expansion valve. *Applied thermal engineering*, 53(1):8–12, 2013.

H. Liu and J. Cai. A robust gray-box modeling methodology for variable-speed direct-expansion systems with limited training data. *International Journal of Refrigeration*, 129:128–138, 2021a.

H. Liu and J. Cai. Improved superheat control of variable-speed vapor compression systems in provision of fast load balancing services. *International Journal of Refrigeration*, 2021b. Accepted.

B. P. Rasmussen. Dynamic modeling for vapor compression systems—part i: Literature review. *HVACR Research*, 18(5):934–955, 2012.

D. I. J. D. T. Reindl and P. S. A. Klein. A semi-empirical method for representing domestic refrigerator/freezer compressor calorimeter test data. *ASHRAE TRANSACTIONS*, 2000.

M. M. Shah. A general correlation for heat transfer during film condensation inside pipes. *International journal of heat and mass transfer*, 22(4):547–556, 1979.

T. N. Tandon, H. K. Varma, and C. P. Gupta. A void fraction model for annular two-phase flow. *International journal of heat and mass transfer*, 28(1):191–198, 1985.

E. Winandy, C. Saavedra, and J. Lebrun. Experimental analysis and simplified modelling of a hermetic scroll refrigeration compressor. *Applied thermal engineering*, 22(2):107–120, 2002.

Y. Xia and S. Deng. The influences of the operating characteristics of an electronic expansion valve (eev) on the operational stability of an eev controlled direct expansion air conditioning system. *International journal of refrigeration*, 69:394–406, 2016.

Y. Xia, Q. Ding, J. S., X. Zhang, and S. Deng. A simulation study on the operational stability of an eev-controlled direct expansion air conditioning system under variable speed operation. *International Journal of Refrigeration*, 103:115–125, 2019.